International Journal of Computer Assisted Radiology and Surgery
https://doi.org/10.1007/s11548-018-1817-4

ORIGINAL ARTICLE

Myocardium segmentation from DE MRI with guided random walks and sparse shape representation

Jie Liu[1] · Xiahai Zhuang[2] · Hongzhi Xie[3] · Shuyang Zhang[3] · Lixu Gu[1]

Received: 12 January 2018 / Accepted: 27 June 2018

Abstract

Purpose For patients with myocardial infarction (MI), delayed enhancement (DE) cardiovascular magnetic resonance imaging (MRI) is a sensitive and well-validated technique for the detection and visualization of MI. The myocardium viability assessment with DE MRI is important in diagnosis and treatment management, where myocardium segmentation is a prerequisite. However, few academic works have focused on automated myocardium segmentation from DE images. In this study, we aim to develop an automatic myocardium segmentation algorithm that targets DE images.

Methods We propose a segmentation framework based on both prior shape knowledge and image intensity. Instead of the strong request of the pre-segmentation of cine MRI in the same session, we use the sparse representation method to model the myocardium shape. Data from the Cardiac MR Left Ventricle Segmentation Challenge (2009) are used to build the shape template repository. The method of guided random walks is used to integrate the shape model and intensity information. An iterative approach is used to gradually improve the results.

Results The proposed method was tested on the DE MRI data from 30 MI patients. The proposed method achieved Dice similarity coefficients (DSC) of $74.60 \pm 7.79\%$ with 201 shape templates and $73.56 \pm 6.32\%$ with 56 shape templates, which were close to the inter-observer difference ($73.94 \pm 5.12\%$). To test the generalization of the proposed method to routine clinical images, the DE images of 10 successive new patients were collected, which were unseen during the method development and parameter tuning, and a DSC of $76.02 \pm 7.43\%$ was achieved.

Conclusion The authors propose a novel approach for the segmentation of myocardium from DE MRI by using the sparse representation-based shape model and guided random walks. The sparse representation method effectively models the prior shape with a small number of shape templates, and the proposed method has the potential to achieve clinically relevant results.

Keywords Delayed enhancement MRI · Myocardium segmentation · Guided random walks · Prior shape modeling · Sparse representation

Introduction

Technical advances in hardware and software developments have led to the increasing clinical use of cardiovascular magnetic resonance imaging (MRI). Kim et al. have demonstrated that delayed enhancement (DE) MRI is an effective and well-validated imaging technique for the detection and assessment of myocardial infarction (MI) [1]. DE images are acquired at a 10–15 min delay after an intravenous administration of gadolinium contrast, and a suppressed signal is obtained in normal myocardium that is hyper-enhanced in infarcted regions [1, 2].

The myocardium viability assessment with DE MRI is important in the diagnosis and treatment of MI. With the segmentation of both the myocardium and infarct region in the DE images, some useful coefficients can be calculated, for example, the transmural extent, which is important in disease management and prognosis. Most of the existing academic works that relate to DE MRI focus on the

✉ Xiahai Zhuang
zxh@fudan.edu.cn

✉ Lixu Gu
gulixu@sjtu.edu.cn

1 School of Biomedical Engineering, Shanghai Jiao Tong University, Shanghai 200240, China

2 School of Data Science, Fudan University, Shanghai 200433, China

3 Department of Cardiothoracic Surgery, Peking Union Medical College Hospital, Beijing 100730, China

Published online: 07 July 2018

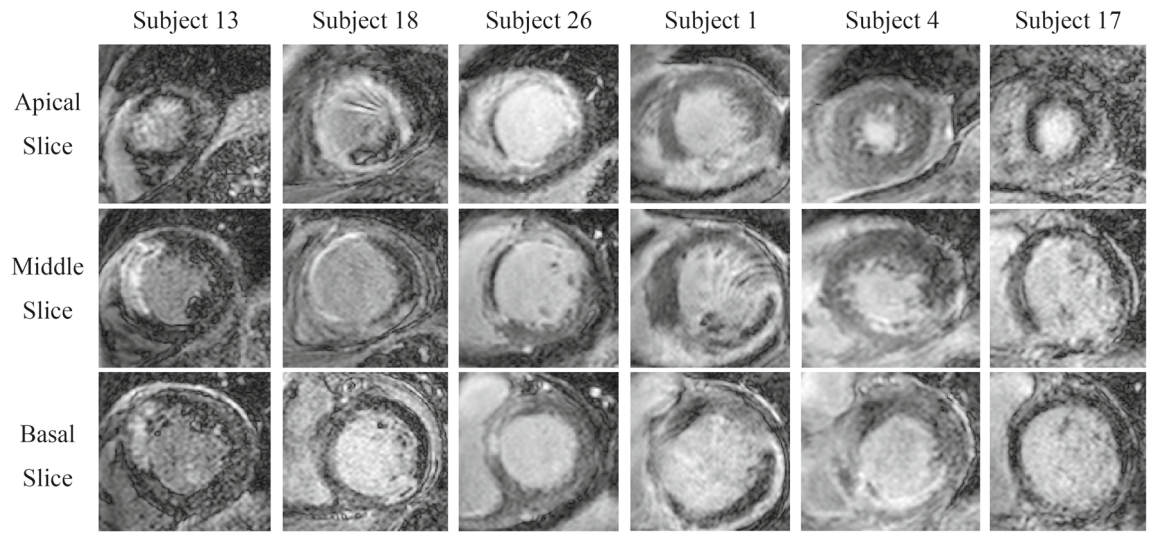

Fig. 1 Examples of the DE images: the apical, middle and basal slices of 6 subjects are shown

automatic localization and quantification of infarct regions, while the delineation of myocardium is assumed to have already been achieved [3–9]. Since the manual segmentation of myocardium is labor-consuming and suffers from inter-observer variations [10], automatic myocardium segmentation is desired. However, obtaining this ambitious goal can be arduous, primarily due to the characteristics of DE images. First, the hyper-enhanced infarcted region and suppressed healthy region result in the heterogeneous intensity of the myocardium. In other MRI sequences, such as the widely used cine MRI, where MI cannot be visualized, a uniform distribution of myocardium intensity is often assumed [11, 12]. Thus, many automatic segmentation methods that are designed and tested on other types of images are challenged. Second, the intensity range of myocardium overlaps with the intensity range of the surrounding tissues [10, 13], and often, no distinct boundary can be observed, as illustrated in Fig. 1. Third, the enhancement patterns are complex. The location, size and shape of the infarcted regions vary significantly from patient to patient. Microvascular obstruction (MVO), which appears as hypo-enhanced areas (because of the lack of contrast agent uptake) within the hyper-enhanced infarcted region [2, 14], can also occur. The introduction of geometric assumptions regarding infarcted regions may actually limit the scope of the applications for the designed algorithm.

Currently, limited work has been performed on myocardial segmentation from DE MRI. Most existing approaches take the myocardial segmentation from cine MRI that is acquired in the same session as *a priori* knowledge, since cine MRI, for which many segmentation methods have been proposed, is widely used in MRI examinations. Myocardial segmentation in DE MRI can be achieved by the direct propagation of segmentation from cine MRI. Different registration methods were designed for this propagation, such as 2D rigid registration based on a shift window [15], affine transformation [16] and rigid registration that incorporates multiscale total variation flow [17]. However, with the non-rigid deformation of the heart and possible errors in the electrocardiography gating during image acquisition, rigid or affine registration may be unable to capture all deformations. In previous academic work [10, 18, 19], an additional process was performed after registering the cine and DE images, where the propagated prior segmentation was deformed toward the myocardium contours in the target DE images. To detect the contours in DE images, Ciofolo et al. proposed a 2D geometrical template, where myocardium was modeled as a closed ribbon structure with an imaginary centerline and variable width [18]. Wei et al. proposed a 1D parametric model to detect paired endocardial and epicardial edge points, where the intensity patterns along the radial rays from the left ventricle (LV) center to beyond the epicardium were modeled [19].

The segmentation results of cine MRI are strong prior information, which can simplify segmentation [19]. However, respiratory motions and differences in the thoracic gas volume between breath holdings can prevent DE and cine MRI from covering the same scope of the heart [10]. In addition, expert supervision can be required in the cine MRI segmentation stage and in the cine and DE MRI registration stage [19], which limits the minimization of human interaction. Some attempts have also been made to segment DE images without the guidance of cine MRI [13, 20, 21]. However, only the epicardium has been segmented [13], and relatively weak prior knowledge of the myocardium thickness constraint has been previously adopted [21], which makes it difficult to guarantee a realistic shape in the results.

In this paper, we propose a segmentation approach toward the DE images to simplify the segmentation procedure and

minimize human supervision. Our work is distinct from the existing methods in three aspects. First, we explore the possibility of eliminating the strong dependency of the pre-segmented cine MRI, and we use a shape model to provide the prior information. Second, to maintain the shape characters of each shape template and achieve sufficient flexibility, we use the sparse representation technique to build the shape model. Third, for the information extraction from the DE images, we adopt a method based on random walks. The prior shape model is also integrated to form the guided random walks.

The rest of this paper is organized as follows. The proposed segmentation framework are described in "Materials and method" section, the validation method and experiment results are presented in "Performance analysis" section, and the discussion and conclusion are in "Discussion" and "Conclusion" sections, respectively.

Materials and method

Data Preparation

We acquired navigated 3D acquisition DE MRI from 30 patients with myocardium infarction as the testing data. The resolution of the DE MRI was $0.7292 \times 0.7292 \times 5$ mm. Each image contained 10–18 short axis slices with 490×490 pixels in each slice. An observer with expertise in cardiac anatomy manually delineated the myocardial boundaries on all the data to generate the "gold standard" for evaluation. Furthermore, for an inter-observer study, we randomly selected 10 subjects from the data for another manual segmentation. This segmentation was performed independently by another expert, who did not have access to the first manual segmentation. ITK-SNAP (www.itksnap.org) was used to perform the manual segmentations [22].

Though cine MRI was not needed in the proposed method, we also collected cine images of the target patients to generate the patient-specific prior shape, for evaluation of the adopted shape model. The resolution of the cine MRI was $1.25 \times 1.25 \times 11$ mm. The automatic segmentation of cine MRI is still an open question; therefore, we used manual segmentation, which provides the best patient-specific prior information. The manual segmentation of cine MRI was performed by the same expert who generated the DE gold standard.

Since the number of our acquired DE data sets is limited, the data from the Cardiac MR Left Ventricle Segmentation Challenge (2009) [23] were downloaded as training data, to obtain the prior shape of the myocardium. Two specific categories of the data were selected, including heart failure with infarct and normal heart. Manual segmentation from the end-diastolic phase of the selected subjects was used for modeling the prior shape, which contains 21 subjects and 201 slices in total.

Automatic Segmentation Framework

An overview of proposed segmentation method is shown in Fig. 2. The method is described in five parts, namely the atlas-based initialization, the construction of target-specific dictionary, the sparse representation-based shape model, the guided random walks and the iterative framework. The emphasis is made on the target-specific dictionary, the sparse shape model and the guided random walks.

Initialization of the Segmentation Algorithm

First, the atlas-based method is used to generate an initial segmentation of the myocardium. The atlas is pre-established from the high-resolution MRI scan of a healthy volunteer and is resampled to the resolution of $1 \times 1 \times 1$ mm. The registration scheme is based on the previous work of Zhuang et al [24]., which consists of three steps, namely global affine registration for the localization of the entire heart, the locally affine registration method for the initialization of substructures and free-form deformation registration based on spatially encoded mutual information [25]. The registration tools can be downloaded from ZXHPROJ (http://www.sdspeople.fudan.edu.cn/zhuangxiahai/0/zxhproj/). The resultant transformation is used to transform the atlas into the image space of the target DE MR image.

Construction of a Target-Specific Dictionary

With the 201 MRI slices from the Challenge data set, a shape template repository can be built. Because of the large slice thickness (i.e., the gap between slices) in DE MRI, the shape information between slices is discontinuous. We therefore use 2D slices as the shape templates. Instead of using the explicit parametric shape representation [26, 27], we represent the manual segmentation of each slice as a mask, where the position of myocardium is marked with 1, and the rest is marked with 0, similar to the method in [28].

Given a target slice, all the shape templates are aligned to the LV center of the target slice, which can be estimated using the initial segmentation. To keep the shape characters and detail information of the original templates, we use rigid registration for this alignment. One can formulate a shape template using a vector $s_i \in \mathbb{R}^k, i = 1, \ldots, N$, where k is the number of pixels in each aligned shape template, and N is the total number of shape templates.

For each target slice, only a small set of the templates resembles the size and shape of the target myocardium. Therefore, using all the templates may not be necessary for an efficient and effective modeling. We therefore pro-

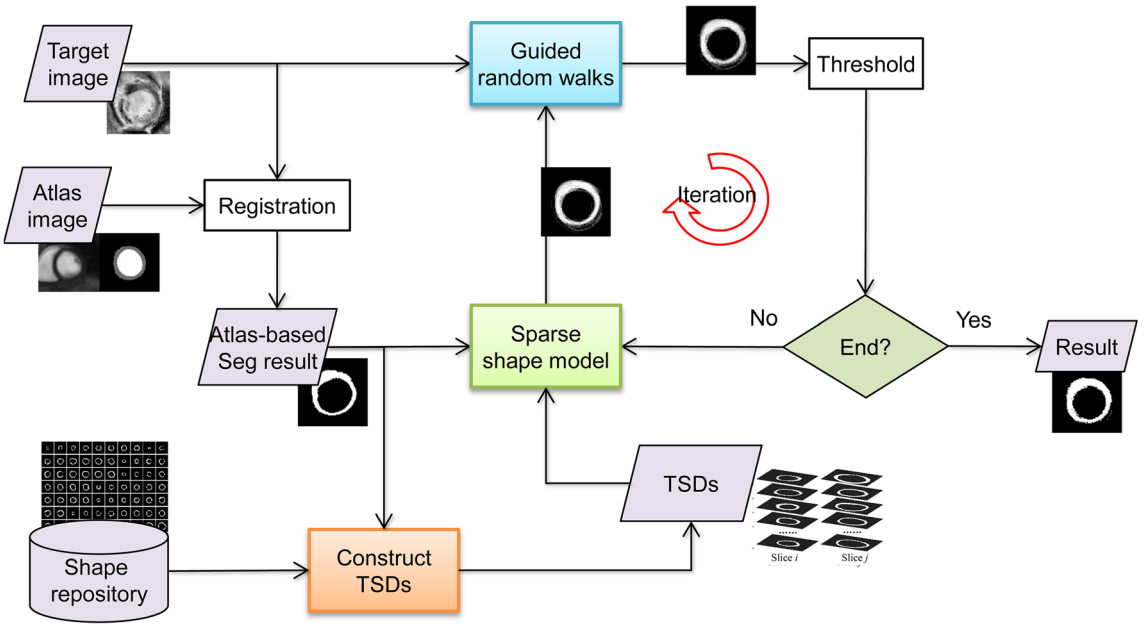

Fig. 2 Flowchart of the proposed method. Three important components are the sparse shape model, guided random walks and the construction of a target-specific dictionary (TSD)

pose to build a target-specific shape dictionary for each slice. Intuitively, the templates that have similar position and myocardial shape to the target should be more important in myocardial shape representation. For example, the templates that are built with apical slices may be less useful in the segmentation of a basal slice. In this work, an empirical method is used. We use the Dice similarity coefficient (DSC) between the templates and the initial segmentation to define the selection criterion such that a template is selected when its DSC exceeds a threshold, for example, 30% in our experiment. The selected templates are then used to construct the target-specific dictionary, $\boldsymbol{D}_r = [\boldsymbol{s}_{r1}, \boldsymbol{s}_{r2}, \ldots, \boldsymbol{s}_{rn}]$, where subscript r represents the r th slice in the target data, and n is the total number of shape templates that are selected for the rth slice. The value of n depends on the number of templates that meet the above DSC criterion, and this value is approximately 60–120 in this study.

Prior Shape Modeling

Because of the indistinct boundaries and complex variability of the heart's shape, prior knowledge is critical to obtain an automatic segmentation result with a realistic heart shape. We model the myocardium shape using a sparse linear combination of the components of the target-specific dictionary $\boldsymbol{D}_r$. The combination coefficient vector $\boldsymbol{\alpha}_r \in \mathbb{R}^{\boldsymbol{n}}$ is determined as follows:

$$\boldsymbol{\alpha}_r = \arg\min_{\boldsymbol{w}} \boldsymbol{y} - \boldsymbol{D}_r \boldsymbol{w}_2^2 + \lambda \boldsymbol{w}_1, \tag{1}$$

where $\boldsymbol{y} \in \mathbb{R}^k$ is the vector that represents the current segmentation of myocardium, and $\boldsymbol{w}$ is the sparse representation coefficient vector. The L1 norm term imposes sparsity, and parameter λ controls the level of sparsity. Intuitively, when parameter λ is larger, fewer nonzero elements will be in vector $\boldsymbol{w}$, that is less templates in $\boldsymbol{D}_r$ will be effective in representing the myocardium. The Lasso problem of Eq. (1) is solved with SPAMS (http://spams-devel.gforge.inria.fr/), where a fast implementation of the least angle regression algorithm is used [29].

Then, the prior shape can be represented as

$$\boldsymbol{y}_r^{\text{shape}} = \boldsymbol{D}_r \boldsymbol{\alpha}_r. \tag{2}$$

Guided Random Walks

To fit the shape model to the target images and achieve the segmentation results, the intensity information in the DE images must also be analyzed. For this purpose, we adopt the random walks method and integrate the prior shape to form the guided random walks.

The method of random walks is a graph-based segmentation algorithm where an image is treated as a graph $G = (V, E)$ with vertex set V and edge set E. Each voxel in the image is represented as a vertex $v \in V$, and each neighboring vertex pair v_i, v_j (e.g., 6- or 26-connected in 3D images) is spanned with an edge $e_{ij} \in E \subseteq V \times V$. A real-valued weight is assigned to each edge, representing the likelihood that a random walker will cross this edge. The algorithm calculates the probability x_i that a random walker, starting at an

unseeded voxel v_i, first reaches the user labeled seeds of a specific class (e.g., myocardium). This problem can be solved by calculating the solution of a system of sparse linear equations. The size of the linear equations depends on the number of voxels in the target image. The random walks algorithm has the pragmatic properties of weak boundary detection, noise robustness and the assignment of ambiguous regions [30].

In this work, instead of using manually labeled seeds as the prior information [30], we use the prior shape to guide the random walks. Given the target image, a 2D prior shape is constructed for each slice, that is, $\boldsymbol{y}_r^{\text{shape}}$ for the rth slice. We denote the prior shape for all the slices with $\boldsymbol{y}^{\text{shape}}$. The energy function is designed as

$$E(\boldsymbol{x}) = \frac{1}{2}\sum_{e_{ij}\in E}\omega_{ij}\left(x_i - x_j\right)^2 + \gamma\cdot\frac{1}{2}\sum_{i\in V}\left(x_i - y_i^{\text{shape}}\right)^2, \tag{3}$$

where x_i represents the probability for myocardium in voxel i, and γ is a weighting parameter. Here, we compute the edge weights based on the intensity difference between the vertices as follows:

$$\omega_{ij} = \exp\left(-\beta\left(I_i - I_j\right)^2\right), \tag{4}$$

where I_i is the image intensity of voxel i, and β is an adjustable parameter that controls the sensitivity to the intensity contrast.

The first term in Eq. (3) is the conventional random walks term. When the neighboring voxels have similar intensities I_i and I_j, the value of the edge weight ω_{ij} is close to 1. Thus, minimizing the first term leads to similar probabilities x_i and x_j. In contrast, when the intensities are different, the weight, ω_{ij}, tends to zero. Then, the probabilities x_i and x_j do not affect one another. The second term is the proposed prior-guided term, which drives the value of x_i toward the value of prior shape y_i^{shape}.

Equation (3) can be rewritten in the matrix form as

$$E(\boldsymbol{x}) = \boldsymbol{x}^T\boldsymbol{L}\boldsymbol{x} + \frac{\gamma}{2}\left(\boldsymbol{x}^T\boldsymbol{x} - 2\boldsymbol{x}^T\boldsymbol{y}^{\text{shape}} + \boldsymbol{y}^{\text{shape}T}\boldsymbol{y}^{\text{shape}}\right), \tag{5}$$

where $\boldsymbol{x}$ is the vector of the probability of all the voxels, and $\boldsymbol{L}$ is the Laplacian matrix that is defined as

$$L_{ij} = \begin{cases} d_i, & i = j \\ -\omega_{ij}, & e_{ij}\in E \\ 0, & \text{otherwise} \end{cases}, \tag{6}$$

$$d_i = \sum_{e_{ij}\in E}\omega_{ij}. \tag{7}$$

One can obtain the solution by solving a system of linear equations as follows:

$$(2\boldsymbol{L} + \gamma\boldsymbol{I})\boldsymbol{x} = \gamma\boldsymbol{y}^{\text{shape}}. \tag{8}$$

Since $\boldsymbol{L}$ is positive semi-definite [30] and the value of parameter γ is positive, the system is positive definite. Therefore, a unique solution is guaranteed. The size of the linear equations is the number of voxels in the region of interest. In our study, this number is 22,500.

Iterative Segmentation

With the initial segmentation, an iterative scheme is constructed. For each slice, the sparse representation coefficient of the associated shape dictionary is updated to fit the current segmentation by solving Eq. (1). In this process, a strong shape regularization is imposed, and the infrequent shapes may take leading roles in the prior shape modeling. Then, the prior shape that is calculated with Eq. (2) is used to guide the random walks, and the probability for myocardium is computed using Eq. (8). A threshold T is experimentally chosen to compute a binary segmentation from the resulting probability. The current results are then added to the prior shape representation for the next iteration. This procedure is repeated until the number of the changed pixel labels is zero or a maximum number of iterations are reached.

Performance analysis

The parameters used in this work were $\lambda = 0.2$, $\gamma = 0.02$, $\beta = 100$, $T = 0.42$, and the maximum number of iterations was 20. For qualitative evaluation, the segmentation results of the basal, middle and apical slices from 3 subjects are demonstrated in Fig. 3, along with the manual segmentation from the two observers. Also, the results of the proposed method were quantitatively evaluated by comparing with the manual delineation by the first observer, which was performed on all the data. And compared methods were designed to evaluate the effectiveness of each part in the proposed method. Moreover, the effects of the size of shape repository and iteration number were studied.

Evaluation metric

We validated our method using 30 MRI data sets from patients with myocardium infarctions. To quantitatively evaluate the proposed method, we used DSC and shape similarity (SS) [31] to compare the segmentation results with the gold standard.

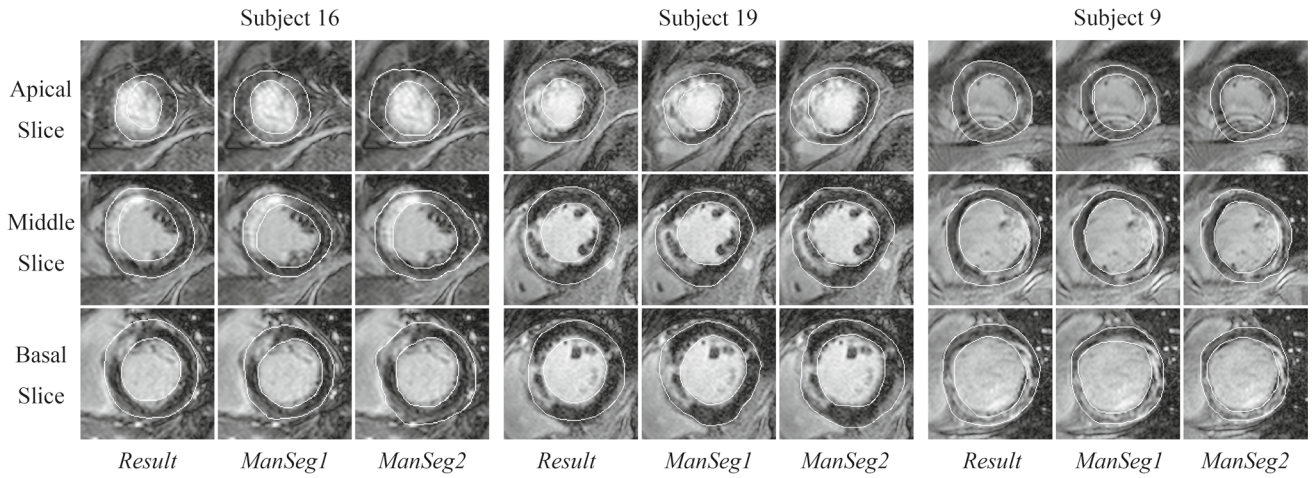

Fig. 3 The automatic and manual segmentation results of three subjects are illustrated: the first column is the results of the proposed method, referred to as "Result"; the second column is the manually delineated gold standard (*ManSeg1*); and the third column is the second manual segmentation for the inter-observer study, referred to as *ManSeg2*

The DSC measures the overlap between the segmentation results $\boldsymbol{y}$ and the gold standard $\boldsymbol{g}$: $\mathrm{DSC}(\boldsymbol{y}, \boldsymbol{g}) = 2|\boldsymbol{y} \cap \boldsymbol{g}|/(|\boldsymbol{y}| + |\boldsymbol{g}|)$.

The SS metric is a function of the angle between the normal vectors of the two boundaries and is weighted by the boundary distance:

$$\mathrm{SS}(\boldsymbol{y}, \boldsymbol{g}) = \frac{1}{|\partial \boldsymbol{g}|} \sum_{n \in \partial \boldsymbol{g}} \left| \frac{|\nabla L_{\boldsymbol{y}}[n] \cdot \nabla L_{\boldsymbol{g}}[n]|}{|\nabla L_{\boldsymbol{y}}[n]||\nabla L_{\boldsymbol{g}}[n]|} \right| \exp\left(-\frac{L_{\boldsymbol{y}}^2[n]}{\sigma^2} \right) \tag{9}$$

where $n \in \partial \boldsymbol{g}$ refers to the boundary points of the gold standard, and $L_{\boldsymbol{y}}[n]$ and $L_{\boldsymbol{g}}[n]$ are the signed distance functions of the boundaries of the segmentation results and the gold standard, respectively. The value of SS is bounded between 0 and 1, and when the value is greater, the two shapes are more similar. A free parameter σ is included in the definition of SS, and its value was set as 10 in our study.

Compared Methods

To evaluate effectiveness of each part in the proposed method, we implemented two simplified versions by removing some important components in the proposed method, that is, the **Atlas** and **AtlasGuided** methods. In the proposed method, the data from the Cardiac MR Left Ventricle Segmentation Challenge (2009) were used to build the shape template repository. These data were acquired from different patients in different environments and were segmented by different people than our testing data. To study the effect of building prior shape using training data from different data center, we designed the **ManGuided** method, where the manual segmentation of corresponding cine images of the target DE data was used to generate the patient-specific prior shape.

Atlas: In the atlas-based segmentation, the atlas is registered to the target image for segmentation propagation [32]. The registration scheme and the atlas are the same as the initialization in the proposed method.

AtlasGuided: this method is a simplified version of the proposed method where the sparse representation-based shape model is removed, that is, the initialization is used to guide the random walks. The effect of the shape model can be evaluated by comparing it with the proposed method.

ManGuided: instead of using shape templates that are built from different patients, this method uses the manual segmentation of the cine MRI of the same subject. Because the cine and DE MRI data have different slice thicknesses, there is no simple correspondence between the cine and DE MRI slices. Therefore, the cine segmentation from all slices of the subject is used to build the patient-specific dictionary. Then, sparse representation is used to guide the random walks in the same way as the proposed method. The initialization is also performed with the same registration scheme as the proposed method.

All of these methods were evaluated with the same data sets, and the parameters were adjusted to achieve the best results for each method. The inter-observer study on 10 randomly selected subjects was also performed to evaluate the potential of the proposed method for clinical use.

For visual comparison of the four methods, the myocardium segmentation results of 7 subjects are shown in Fig. 4. The DSC and SS of the proposed and compared methods are shown in Table 1. To better illustrate the results, the box plots of the DSC and SS are shown in Fig. 5. The paired t test demonstrated that significant differences exist

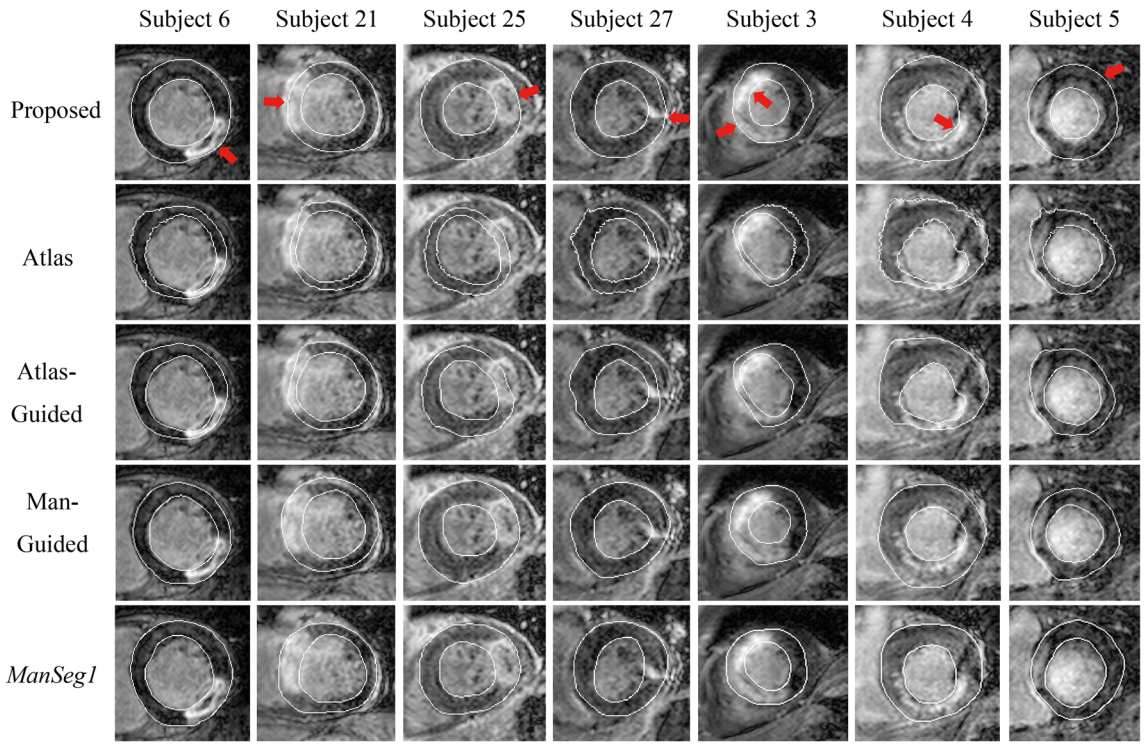

Fig. 4 Visualization of the seven segmentation results of the four methods and the manual segmentation of the first observer, which is taken as gold standard

Table 1 Segmentation accuracy evaluated with DSC (%) and similarity (%)

	Proposed	Atlas	AtlasGuided	ManGuided	Inter-observer
DSC	74.60 ± 7.79	65.22 ± 8.24	71.91 ± 7.51	74.51 ± 8.44	73.94 ± 5.12
SS	79.92 ± 5.88	76.92 ± 6.98	77.86 ± 6.18	79.86 ± 5.94	83.42 ± 4.67

Note that the inter-observer difference is evaluated with 10 data sets

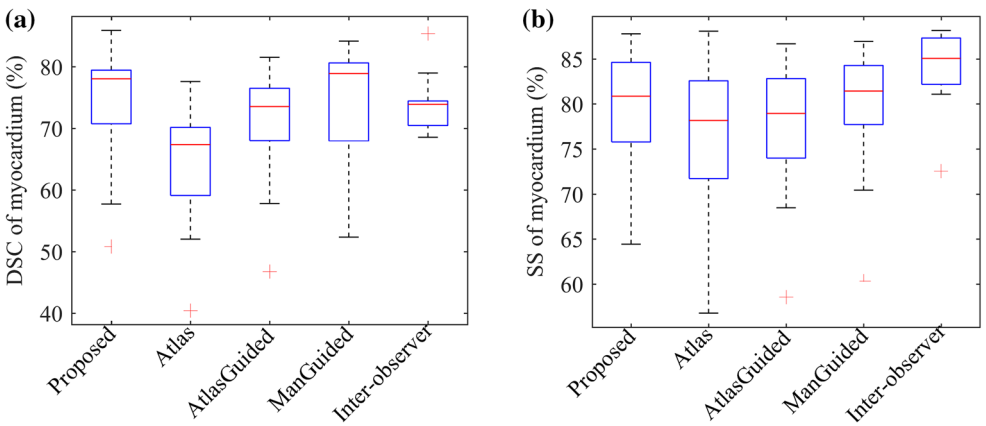

Fig. 5 Box plots of myocardial segmentation results: **a** DSC and **b** SS

between the myocardium DSC of the proposed method and the **Atlas**, **AtlasGuided** methods ($p < 0.01$). No significant difference was detected between the proposed method and the **ManGuided** method.

Method's generalization to unseen data

To test the generalization of the proposed method to routine clinical images, we have collected the DE images of 10 successive new patients. These data were unseen during

Table 2 Effect of selection of shape templates evaluated with DSC (%)

	21 data sets	12 data sets	6 data sets
DSC	74.60 ± 7.79	73.75 ± 6.84	73.56 ± 6.32
SS	79.92 ± 5.88	79.23 ± 5.91	78.60 ± 5.59

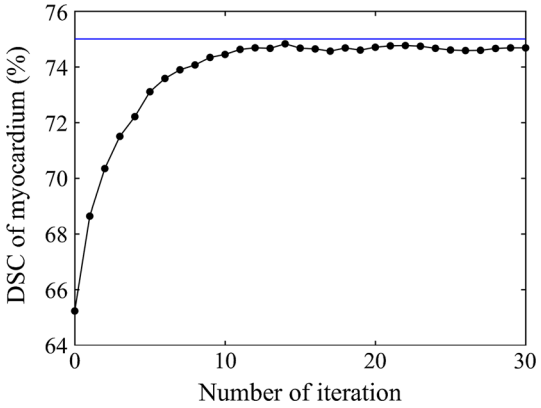

Fig. 6 Effect of iteration number. The blue line indicates the DSC of 75%

the method development and parameter tuning. The results for the 10 new images are: 76.02 ± 7.43% for DSC and 82.15 ± 4.93% for SS.

Effect of Size of Shape Template Repository

We tested the effects using the sets of shape templates with different sizes, including 21 data sets (201 slices), 12 data sets (118 slices) and 6 data sets (56 slices). Table 2 presents the DSC using the three sets of the shape templates.

Effect of Iteration Number

To study the effects of the number of iterations, we recorded the average DSC with respect to different iteration steps, as shown in Fig. 6. The DSC begins to converge when the number of iteration steps reaches 13.

Our program was built on MATLAB and run on a personal computer that is equipped with a Pentium Dual-Core CPU E5200 2.50 GHz and a Kingston 2 GB DDR2 800 MHz RAM. The average runtime was calculated for DE data from one patient, of which the average number of slices is 15. The runtime for atlas-based initialization was 6.03 ± 1.60 min, and that for each iteration was 20.61 ± 4.62 s. If the number of iteration is set at 20, the total time for fully automatically segmentation process is about 13 min. Set a higher value of the threshold for selecting shape templates can reduce the runtime. In our study, when the threshold is set as 0.6, the runtime of each iteration is decreased to 7.55 ± 1.83 s, and the total time can be reduced to about 9 min. Note that the atlas-based initialization can be easily replaced with other techniques, for example the convolution neural network based method [33]. In this kind of methods, when enough training data are provided, the initialization for an unseen data can be done within seconds.

Discussion

As shown in Fig. 3 and the first row in Fig. 4, though no intensity model has been adopted to explicitly model heterogeneous intensity, the random walks method successfully labels both healthy tissue and infarct region as myocardium, regardless of the position and size of the infarction. For indistinct boundaries, once the shape model guides the search to a place near the real boundaries, the random walks method can stop at weak boundaries.

Because of the existence of infarcts and the low intensity contrast, the **Atlas** method tends to make mistakes, especially in the infarcted areas, as demonstrated in the second row of Fig. 4. In the **AtlasGuided** method, where no shape regularization is adopted, these mistakes cannot be corrected, so the infarcts are not marked as likely being myocardium. Thus, the infarcts cannot be classified properly in the **AtlasGuided** method. However, in clinical applications, the objective is the quantitative evaluation of the MI. Therefore, the infarcted region should be the focus of attention. The first row in Fig. 4 shows that, in the proposed method, with the adoption of the sparse representation-based shape method, the delineation of the myocardium is greatly improved, especially in the infarction area, which is indicated with the red arrows. The increase in the mean DSC of the myocardium is relatively small (DSC: proposed: 74.60 ± 7.79%; **AtlasGuided**: 71.91 ± 7.51%), which is likely because the improved region is diluted by the entire volume of the myocardium. Therefore, we believe that our results will have more reference value in clinical assessments.

In the proposed method, the manual segmentation of cine images from a public data set is used to generate the shape templates. In the **ManGuided** method, the cine MRI was acquired during the same session, and manual segmentation was performed by the same expert as the DE gold standard. However, as Table 1 demonstrates, the **ManGuided** method achieves a similar myocardium DSC (74.51 ± 8.44%) to the proposed method (74.60 ± 7.79%), which reveals that the sparse representation in our proposed framework is efficient for prior shape modeling. The shape model provides comparable shape regulation with the manual segmentation of cine MRI of the same patient.

The results in Table 2 demonstrate that a relatively small set of shape templates can effectively represent the myocardium shapes. The results in Table 2 together with that of the **ManGuided** method demonstrate that the shape template repository can be built with a small data set from

Table 3 The results reported in the literature

Reference	No. of patients	DSC (%)		
		Endo	Epi	Myo
Engan et al. [13]	54	N/A	86 ± 0.27	N/A
Wei et al. [19]	21	95.33 ± 3.63, 92.64 ± 4.36	96.88 ± 1.84, 94.35 ± 2.70	88.57 ± 4.75, 82.32 ± 5.59
Tao et al. [10]	50	N/A	N/A	81 ± 7 83 ± 9
Kurzendorfer et al. [20]	26	85 ± 6	84 ± 6	N/A
Liu et al. [21]	22	86.74 ± 5.82	90.40 ± 3.17	73.77 ± 5.56
Proposed	30	85.07 ± 5.79	90.27 ± 3.59	74.60 ± 7.79

Note that Wei et al. [19] and Tao et al. [10] evaluated the results with two sets of manual segmentations. Endo, Epi and Myo represent endocardium, epicardium and myocardium, respectively

different data centers, which greatly extends the application scenarios of the proposed method. In previous work [31], the guided random walks were also used for myocardium segmentation in cine MRI. However, this work adopts a retrieval framework, which is based on the assumption that the training data should have similar cases as the target subject, which requires a relatively large data repository.

The DSC of the proposed method ($74.60 \pm 7.79\%$) is comparable to the inter-observer study ($73.94 \pm 5.12\%$), which indicates that the proposed method has the potential to achieve clinically relevant results. However, it is worth notice that the SS of the proposed method ($79.92 \pm 5.88\%$) is below that of the inter-observer study ($83.42 \pm 4.67\%$). These results reveal that the manual segmentation from different experts is more likely to have similar general shape. The SS of the **ManGuided** method ($79.86 \pm 5.94\%$) does not show any improvement compared to the proposed method. This is probably because that the target DE images may not be acquired at the exact end-diastolic phase as the phase chosen from corresponding cine MRI.

The proposed method achieves DSC of $76.02 \pm 7.43\%$ and SS of $82.15 \pm 4.93\%$ on the 10 new unseen images, which is comparable to the results of the original 30 data. Though the number of unseen data is relative small, the results can add some strength to the algorithm's generalization to routine clinical images, and the robustness against the chosen parameters.

There are totally five parameters in the proposed method. Among these parameters, the threshold T, which is used to generate the binary segmentation from probability map, critically affects the results, especially for target with small number of pixels. In the application for myocardium segmentation, the recommended value range is 0.36–0.44. The rest of four parameters do not have significant effect to the results in relative large value ranges, and the recommended value ranges are: the weighting parameter of shape guided term $0.01 < \gamma < 0.64$, the threshold to select shape templates in the target-specific dictionary 0.3–0.6, the parameter in the Gaussian weighting function $\beta > 100$, the sparsity level parameter $0.1 < \lambda < 1$. Further details about each parameter are provided in "Appendix B."

Comparison with related works

We list the segmentation results of DE MRI reported in the literature in recent years for reference, as summarized in Table 3. However, with the difference in data sets, it is difficult to perform comparison across different studies. In the work of Wei et al. [19] and Tao et al. [10], the corresponding cine MRI is semi-automatically segmented and used as the prior information. In the work of Wei et al., the manual registration is also introduced when the automatic translational registration failed. By contrast, our approach is fully automatic. In these works, the inter-observer study is also performed. The myocardium DSC between two manual segmentations is $82.93 \pm 5.28\%$ [19] and $81 \pm 6\%$ [10], which is much higher than that in our work. This may suggest that the degree of difficulty for myocardium segmentation is different with different data sets.

For the work of Kurzendorfer et al. [20], no prior shape information is used, and weak shape information of myocardium thickness constraint is used in the work of Liu et al. [21]. In the work of Engan et al. [13], only epicardium is segmented. In these works, a realistic shape is not guaranteed in the results.

Possible applications and future work

In practice, myocardium can first be segmented in a DE image with the proposed method. Once the myocardium area has been determined, the segmentation and quantification of infarct regions can be achieved, as many researchers

have reported [3–9]. With the segmentation of both the myocardium and infarct region in DE images, some coefficients can be calculated.

In this work, a simple empirical method is used to build the target-specific shape dictionary. More mathematically sound methods can be used to a build a complete dictionary. Moreover, we found it particularly challenging to further improve the accuracy of myocardium delineation with only information from DE MRI because of the low contrast of DE images and the complex infarct patterns. In clinical practice, DE and T2 MRI are usually analyzed simultaneously to evaluate the MI and edematous regions. In future works, we will attempt to combine the complementary information from the T2 and DE MRI within a unified framework and then simultaneously perform myocardium segmentation on the two sequences. Also, we will try to introduce the constraints along the slices in the future work.

Conclusion

We propose a novel framework for the segmentation of myocardium from DE MRI using prior shape knowledge and image intensity information. Sparse representation is used to model the prior shape with a set of shape templates from different subjects instead of the segmentation of cine MRI in the same session. The method of guided random walks is used to integrate the prior shape and intensity information in DE images. The proposed method adopts an iterative scheme to regularize and optimize the segmentation results. The results show that the proposed method has the potential to achieve clinically relevant results, with an average DSC that is comparable to the inter-observer difference.

Acknowledgements This research is supported by the National Key Research and Development Program (2016YFC0106200), the 863 National Research Fund (2015AA043203), the Science and Technology Commission of Shanghai Municipality (17JC1401600) and the National Nature Science Foundation of China (61190120, 61190124, 61271318, 81301283 and 81511130090).

Compliance with Ethical Standards

Conflict of interest The authors declare that they have no conflict of interest.

Ethical approval For this type of study formal consent is not required. The testing data were collected at our institution with approval from the institutional review board.

Informed consent This article does not contain any studies with human participants or animals performed by any of the authors.

Appendix A: Some explanation about the derivation of solution equation

The energy function in Eq. (5) can be written as:

$$E(\boldsymbol{x}) = \boldsymbol{x}^T \boldsymbol{L}\boldsymbol{x} + \frac{\gamma}{2}\left(\boldsymbol{x}^T\boldsymbol{x} - 2\boldsymbol{x}^T \boldsymbol{y}^{\text{shape}} + \boldsymbol{y}^{\text{shape}T}\boldsymbol{y}^{\text{shape}}\right)$$
$$= \boldsymbol{x}^T\left(\boldsymbol{L} + \frac{\gamma}{2}\boldsymbol{I}\right)\boldsymbol{x} - \gamma\boldsymbol{x}^T\boldsymbol{y}^{\text{shape}} + \frac{\gamma}{2}\boldsymbol{y}^{\text{shape}T}\boldsymbol{y}^{\text{shape}},$$

where $\boldsymbol{x}$ is the vector of the probability of all the voxels; $\boldsymbol{y}^{\text{shape}}$ is the prior shape for all the slices; $\boldsymbol{L}$ is the Laplacian matrix, as defined in Eqs. (6) and (7).

Since $\boldsymbol{L}$ is positive semi-definite and the value of parameter γ is positive, the matrix $\left(\boldsymbol{L} + \frac{\gamma}{2}\boldsymbol{I}\right)$ is positive definite. So the only critical points of $E(\boldsymbol{x})$ will be the minima. Differentiating $E(\boldsymbol{x})$ with respect to $\boldsymbol{x}$, and the minimizer of $E(\boldsymbol{x})$ is given by the linear equations in Eq. (8). By solving this system of linear equations, the probability map of myocardium can be obtained.

Appendix B: The effects of parameters and the recommended value ranges

There are totally five parameters in the proposed method, as summarized in Table 4. Among these parameters, the threshold T, which is used to generate the binary segmentation from probability map, critically affects the results. We have recorded the DSC of myocardium with the threshold T increasing from 0.3 to 0.5, and the results are demonstrated in Fig. 7. The highest average DSC is achieved when the threshold is between 0.4 and 0.42, which contradicts to the convention of setting the threshold at 0.5 for probability binarization. This result is probably due to the elongated shape and relative small area of myocardium, as well as the relative low intensity contrast between myocardium and surrounding tissues. Since there is a neighborhood-related term in the energy function of random walks method, the probabilities of myocardium are easily affected by the pixels of background, including the blood pool encountered by the endocardium and the tissues around the epicardium. Therefore, a threshold below 0.5 is helpful to prevent the myocardium from being "swallowed" by the background. Evaluated with our testing data sets, when the threshold decreases from 0.4, the DSC decreases slowly because of the tendency to wrongly classify the surrounding pixels into myocardium. When the threshold increases to 0.48, in some data sets, the myocardium begins to be incorporated into the background, which results in a low average DSC and high DSC variance. When the method is applied for myocardium segmentation and the data resolution is similar to our data sets, this value does not need to be changed. When the segmentation target is of larger pixel number, such as in the case of data with higher resolution or

Table 4 The parameters in the proposed method

Parameter	Representation	Recommended value range
T	Threshold used to generate the binary segmentation from probability map	0.36–0.44
γ	Weighting parameter of shape guided term	0.01–0.64
T_D	Threshold to select shape templates in the target-specific dictionary	0.3–0.6
β	Parameter in the Gaussian weighting function	>100
λ	Sparsity level parameter	0.1–1

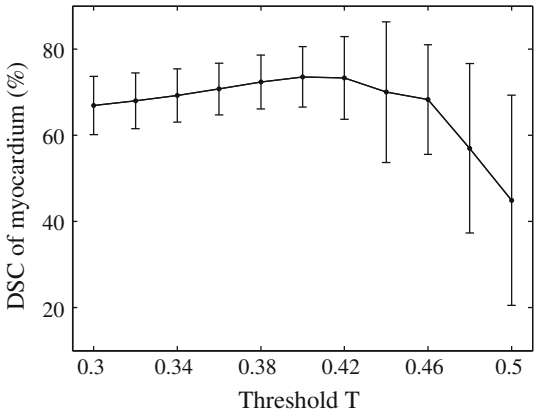

Fig. 7 Effect of threshold T

target tissue of larger area, the value of threshold T will have less effect to the results.

The rest of four parameters do not have significant effect to the results in relative large value ranges. We have recorded the DSC of myocardium with weighting parameter γ doubling from 0.005 to 0.64, as illustrated in Fig. 8. The highest average DSC is achieved when γ is set at 0.01, but the paired t test shows that no significant difference ($p < 0.05$) exists between the γ value of 0.01 and the rest. This demonstrates that the change of parameter γ in a relatively large range (from 0.005 to 0.64) does not have a great effect on the final segmentation results. When the value of parameter γ is small, such as 0.005, insufficient shape information is imposed and the performance of the method becomes less stable, where the DSC standard deviation is larger. When parameter γ is set at a large value, such as 0.64, the imposed constraint may limit the flexibility of the algorithm, which results in a poorer fitting of the results to the image intensity.

The sparse representation-based model is able to select the proper shape templates from the dictionary to model the myocardium shape. However, as the size of the dictionary increase, the computation time will also increase. So

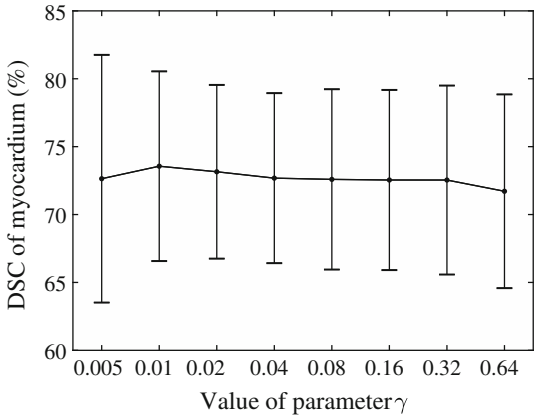

Fig. 8 Effect of weighting parameter γ

we proposed to build the target-specific dictionary, where a threshold of DSC is used to remove some irrelevant shape templates and reduce the size of the dictionary. The shape repository used in this study is relative small, so we choose a low threshold of 30%. In this study, with the shape template repository built with 201 slices from the Challenge data set, a threshold below 50% does not have effect to the accuracy of results. And with a threshold of 60%, a DSC of $73.15 \pm 8.50\%$ is achieved. When the threshold is further increased, for some slices, no shape templates will be kept or the reserved number is too small to give enough flexibility modeling the actual myocardium shape. In the clinical practice, in order to reduce the computation time, the value can be set higher (such as 50–60%). Also, if the shape repository is large and has a good variety of shape characters, a higher value should be set.

The parameter λ in the sparse representation-based shape model controls the level of sparsity. When the parameter λ is larger, the nonzero elements in the vector $\boldsymbol{w}$ will be less. This means that less templates in D_r will be effective in representing the myocardium. In this study, the value of λ changing between 0.1–1 does not have significantly effect to the results.

Another free parameter is β in the Gaussian weighting function. When the value of β increases, the sensitivity of the random walks method to the intensity contrast increases. In our empirical observations, when the value of β is sufficiently large, changing β in a large range does not affect the results. In our experiment, the square gradients are normalized to the interval of [0, 1], and good results can be achieved when $\beta > 100$. In a relevant work [31], a careful study of the effect of β was undertaken, and a similar trend was found.

References

1. Kim HW, Farzaneh-Far A, Kim RJ (2009) Cardiovascular magnetic resonance in patients with myocardial infarction: current and emerging applications. J Am Coll Cardiol 55(1):1–16

2. Beek AM, van Rossum AC (2010) Cardiovascular magnetic resonance imaging in patients with acute myocardial infarction. Heart 96(3):237–243
3. Flett AS, Hasleton J, Cook C, Hausenloy D, Quarta G, Ariti C, Muthurangu V, Moon JC (2011) Evaluation of techniques for the quantification of myocardial scar of differing etiology using cardiac magnetic resonance. JACC Cardiovasc Imaging 4(2):150–156
4. Metwally MK, El-Gayar N, Osman NF (2010) Improved technique to detect the infarction in delayed enhancement image using k-mean method. In: Campilho A, Kamel M (eds) Image analysis and recognition. Springer, Berlin, pp 108–119. https://doi.org/10.1007/978-3-642-13775-4_12
5. Valindria VV, Angue M, Vignon N, Walker PM, Cochet A, Lalande A (2011) Automatic quantification of myocardial infarction from delayed enhancement MRI. In: 7th international conference on signal-image technology and internet-based systems (SITIS). IEEE, pp 277–283
6. Elagouni K, Ciofolo-Veit C, Mory B (2010) Automatic segmentation of pathological tissues in cardiac MRI. In: IEEE international symposium on biomedical imaging: from nano to macro (ISBI). IEEE, pp 472–475
7. Hennemuth A, Seeger A, Friman O, Miller S, Klumpp B, Oeltze S, Peitgen H-O (2008) A comprehensive approach to the analysis of contrast enhanced cardiac MR images. IEEE Trans Med Imaging 27(11):1592–1610
8. Hennemuth A, Friman O, Huellebrand M, Peitgen H-O (2012) Mixture-model-based segmentation of myocardial delayed enhancement MRI. In: Camara O, Mansi T, Pop M, Rhode K, Sermesant M, Young A (eds) Statistical atlases and computational models of the heart. Imaging and modelling challenges. Springer, Berlin, pp 87–96. https://doi.org/10.1007/978-3-642-36961-2_11
9. Tao Q, Milles J, Zeppenfeld K, Lamb HJ, Bax JJ, Reiber JH, van der Geest RJ (2010) Automated segmentation of myocardial scar in late enhancement MRI using combined intensity and spatial information. Magn Reson Med 64(2):586–594
10. Tao Q, Piers SRD, Lamb HJ, van der Geest RJ (2015) Automated left ventricle segmentation in late gadolinium-enhanced MRI for objective myocardial scar assessment. J Magn Reson Imaging 42(2):390–399. https://doi.org/10.1002/jmri.24804
11. Queirós S, Barbosa D, Heyde B, Morais P, Vilaça JL, Friboulet D, Bernard O, D'hooge J (2014) Fast automatic myocardial segmentation in 4D cine CMR datasets. Med Image Anal 18(7):1115–1131. https://doi.org/10.1016/j.media.2014.06.001
12. Liu Y, Captur G, Moon JC, Guo SX, Yang XP, Zhang SX, Li CM (2016) Distance regularized two level sets for segmentation of left and right ventricles from cine-MRI. Magn Reson Imaging 34(5):699–706. https://doi.org/10.1016/j.mri.2015.12.027
13. Engan K, Naranjo V, Eftesol T, Orn S, Woie L (2013) Automatic segmentation of the epicardium in late gadolinium enhanced cardiac MR images. Paper presented at the computing in cardiology conference
14. Wu KC, Zerhouni EA, Judd RM, Lugo-Olivieri CH, Barouch LA, Schulman SP, Blumenthal RS, Lima JAC (1998) Prognostic significance of microvascular obstruction by magnetic resonance imaging in patients with acute myocardial infarction. Circulation 97(8):765–772. https://doi.org/10.1161/01.cir.97.8.765
15. El-Berbari R, Kachenoura N, Frouin F, Herment A, Mousseaux E, Bloch I (2009) An automated quantification of the transmural myocardial infarct extent using cardiac DE-MR images. In: Conference proceedings of IEEE engineering in medicine and biology society, pp 4403–4406
16. Dikici E, O'Donnell T, Setser R, White RD (2004) Quantification of delayed enhancement MR images. In: Medical image computing and computer-assisted intervention (MICCAI). Springer, pp 250–257
17. Xu RS, Athavale P, Lu Y, Radau P, Wright GA (2013) Myocardial segmentation in late-enhancement MR images via registration and propagation of cine contours. In: IEEE 10th international symposium on biomedical imaging (ISBI). IEEE, pp 856–859
18. Ciofolo C, Fradkin M, Mory B, Hautvast G, Breeuwer M (2008) Automatic myocardium segmentation in late-enhancement MRI. In: 5th IEEE international symposium on biomedical imaging: from nano to macro (ISBI). IEEE, pp 225–228
19. Wei D, Sun Y, Ong S-H, Chai P, Teo LL, Low AF (2013) Three-dimensional segmentation of the left ventricle in late gadolinium enhanced MR images of chronic infarction combining long-and short-axis information. Med Image Anal 17(6):685–697
20. Kurzendorfer T, Brost A, Forman C, Maier A (2017) Automated left ventricle segmentation in 2-D LGE-MRI. In: IEEE 14th international symposium onbiomedical imaging (ISBI), pp 831–834
21. Liu J, Zhuang X, Wu L, An D, Xu J, Peters T, Gu L (2017) Myocardium segmentation from DE MRI using multi-component gaussian mixture model and coupled level set. IEEE Trans Biomed Eng 64(11):2650–2661. https://doi.org/10.1109/TBME.2017.2657656
22. Yushkevich PA, Piven J, Hazlett HC, Smith RG, Ho S, Gee JC, Gerig G (2006) User-guided 3D active contour segmentation of anatomical structures: significantly improved efficiency and reliability. Neuroimage 31(3):1116–1128. https://doi.org/10.1016/j.neuroimage.2006.01.015
23. Radau P, Lu Y, Connelly K, Paul G, Dick A, Wright G (2009) Evaluation framework for algorithms segmenting short axis cardiac MRI. MIDAS J 49(6)
24. Zhuang X, Rhode KS, Razavi RS, Hawkes DJ, Ourselin S (2010) A Registration-Based Propagation Framework for Automatic Whole Heart Segmentation of Cardiac MRI. IEEE Trans Med Imaging 29(9):1612–1625. https://doi.org/10.1109/TMI.2010.2047112
25. Zhuang XH, Arridge S, Hawkes DJ, Ourselin S (2011) A nonrigid registration framework using spatially encoded mutual information and free-form deformations. IEEE Trans Med Imaging 30(10):1819–1828. https://doi.org/10.1109/Tmi.2011.2150240
26. Cootes TF, Taylor CJ, Cooper DH, Graham J (1995) Active shape models-their training and application. Comput Vis Image Underst 61(1):38–59
27. Zhang S, Zhan Y, Dewan M, Huang J, Metaxas DN, Zhou XS (2012) Towards robust and effective shape modeling: sparse shape composition. Med Image Anal 16(1):265–277
28. Liu W, Ruan D Segmentation with a shape dictionary. In: IEEE 11th international symposium on biomedical imaging (ISBI), 2014. IEEE, pp 357–360
29. Efron B, Hastie T, Johnstone I, Tibshirani R (2004) Least angle regression. Ann Statist 32(2):407–499. https://doi.org/10.1214/009053604000000067
30. Grady L (2006) Random walks for image segmentation. IEEE Trans Pattern Anal Mach Intell 28(11):1768–1783
31. Eslami A, Karamalis A, Katouzian A, Navab N (2013) Segmentation by retrieval with guided random walks: application to left ventricle segmentation in MRI. Med Image Anal 17(2):236–253
32. Zhuang XH, Shen J (2016) Multi-scale patch and multi-modality atlases for whole heart segmentation of MRI. Med Image Anal 31:77–87. https://doi.org/10.1016/j.media.2016.02.006
33. Pop M, Sermesant M, Jodoin P-M, Lalande A, Zhang X, Yang G, Young A, Bernanrd O (eds) (2017) Statistical Atlases and computational models of the heart. ACDC and MMWHS challenges, vol 10663. Springer, Berlin. https://doi.org/10.1007/978-3-319-75541-0